Int. J. Electrochem. Sci., 17 **(2022)** Article Number: 220236, doi: 10.20964/2022.02.38

International Journal of
ELECTROCHEMICAL
SCIENCE
www.electrochemsci.org

A Theoretical Model for Metal Cation Reduction in the Flow Field and Its Application to Copper Electrorefining

Wenyu Feng, Huazhen Cao, YuKun Shen, Shenghang Xu, Huibin Zhang, Guoqu Zheng**

College of Materials Science and Engineering, Zhejiang University of Technology, Hangzhou 310014, China
*E-mail: zhenggq@zjut.edu.cn, caohz@zjut.edu.cn

Received: 24 November 2021 / *Accepted:* 21 December 2021 / *Published:* 5 January 2022

This paper studies the kinetic process of cation discharge in the flow field of a forced-flowing electrolyte during copper electrorefining. Through electrochemical methods such as rotating disk electrodes, linear sweep voltammetry curves and cathodic polarization curves, the diffusion coefficient (D), reaction rate constant (k^0), transfer coefficient (α) and other electrochemical parameters were obtained. A theoretical model revealing the mass transfer and discharge process of cations in the copper electrolyte was established. This model can be used to analyze the reduction behavior of Cu^{2+} and Bi^{3+} at the surface of the cathode and give the theoretical influence of various electrolysis factors on the purity of the cathode copper. The actual electrorefining experiments confirmed that the variation regularity of copper purity is consistent with the theoretical model. Meanwhile, optimized copper electrorefining experiments were conducted in the simulated industrial electrolyte according to theoretical analysis results with high impurity concentration, by which the purity of the cathode copper reached 99.995%.

Keywords: copper electrorefining, diffusion coefficient, flow field, theoretical model

1. INTRODUCTION

With the rapid development of copper smelting technology, flash smelting [1, 2] and bath smelting [3, 4] processes are widely used in copper pyrometallurgy. Despite the fast smelting speed and high intensity of these methods, they have a weak purification ability [5, 6]. At the same time, due to the gradually decreasing grade of copper ore [7], the content of impurities such as arsenic, antimony, bismuth, iron and lead in the ore is gradually increasing, resulting in a higher content of impurities in anode copper smelted by these processes [8]. In the copper electrorefining process, the concentration of these detrimental impurities dissolved from the anode copper to the electrolyte increases and negatively impacts the quality of the cathode copper, seriously even endangers the entire electrolytic system [9-11].

By means of electrolyte purification, As, Sb, Bi and other impurities can be removed to reduce their inclusion and deposition in the cathode and obtain a cathode copper with a higher purity [12, 13]. However, with the elevated content of these impurities in the electrolyte, the production load and treatment cost of the purification process also increases. To solve this problem, researchers proposed technology such as cyclone electrolysis [14, 15], parallel flow electrolysis [16] and side flow electrolysis [17], which force the electrolyte into a forced flow state and improve the mass transfer of copper in the electrorefining process to effectively reduce the frequency of electrolyte purification without affecting the preparation of a high-purity cathode copper. However, current research is mainly focused on the exploration of electrolyte flow technology; the mass transfer process and concentration variation law of cations on the cathode surface have not been studied in detail.

In the flow field of a forced-flowing electrolyte, the diffusion coefficient, reaction rate constant, exchange current density and transfer coefficient of the cation reduction process can be determined by the RDE technique [18,19], which reveals the law of cation mass transfer on the electrode surface and the kinetic process of reduction. For example, Volgin [20] studied the influence of complex formation onmass transfer in a solution containing three types of ions (metal cations, cation complexes and nonelectroactive anions) on a rotating disk electrode and clarified the concentration distribution of these ions near the electrode surface. Diaz [21] obtained a mathematical model of the behavior of ammonia electrooxidation on a rotating platinum disk electrode through a micro kinetics approach. For the copper electrorefining process, Taina [22] used a rotating disk electrode to measure the diffusion coefficient of copper in the electrolyte, so as to qualitatively analyze the difficulty of Cu^{2+} reduction and the energy consumption of the copper electrorefining process. David [23] proposed a model which can elucidate the influence of solution composition, transport properties, kinetic constants, and convective flow on current distribution and polarization characteristics in the process of copper electrorefining with the assistant of diffusion coefficient and other kinetic parameters. However, they didn’t clarify a quantitative model for the reduction rate of cations at the cathode. Meantime, the influence of impurity ions on the reduction behavior of copper ions and product purity in actual electrorefining has not yet been explored. Simultaneously, there are few completed theoretical explanations for why the forced flow system can effectively improve the purity of cathode copper.

In this paper, a rotating disk electrode was used to investigate the diffusion coefficients and other electrochemical parameters of Cu^{2+} and Bi^{3+} in the copper electrorefining process under different temperatures, H_2SO_4 concentrations, electrode speeds and other conditions. Combined with the diffusion layer theory and the mass transfer rate equation, our findings were used to establish a mathematical model indicating the influence of different temperatures, acidities, speeds and other conditions on the reduction reaction rate of Cu^{2+} and Bi^{3+} in the flow field of a forced-flowing electrolyte. This model can be used to reveal the concentration change and reduction behavior of Cu^{2+} and Bi^{3+} in the copper electrorefining process and the effect of different electrolytic conditions on the purity of copper. And the model can also be well applied in the actual copper electrorefining process, only need to substitute the corresponding cation concentration, temperature and other parameters to this model, the reduction rate of Cu^{2+} and other impurity cations can be effectively predicted, so as to obtain the best electrorefining conditions in advance.

2. EXPERIMENTAL

2.1 Electrolyte preparation

Analytical grade sulfuric acid (H_2SO_4, ≥98%), copper(II) sulfate pentahydrate (≥99%), and bismuth oxide (≥99%) were used to prepare the copper electrolyte and bismuth electrolyte. All aqueous solutions were freshly prepared with deionized water. In this work, an electrolyte with a composition similar to that of an industrial electrolyte was prepared for experiments to verify the applicability of the model. Before each experiment, high-purity argon was blown into the electrolyte for 15 minutes to remove dissolved oxygen. During the experiment, 30 mL of the electrolyte was placed in a 50 mL electrolytic cell, and the temperature was kept constant by a water bath. All tests were carried out between 313 and 333 K.

2.2 Electrochemical test and analysis

Linear sweep voltammetry curves (LSV) were measured on a CHI660C electrochemical workstation (CH Instrument, Shanghai, China). The working electrode was a rotating glassy carbon electrode (ATA-1B, Jiangsu Jiangfen, China), the counter electrode was a platinum wire, and the reference electrode was a saturated calomel electrode (SCE). The glassy carbon electrode was mechanically polished with wet alumina powder (0.05 to 0.3 μm). During the tests, the rotation speed of the working electrode was 100, 200, 300, 400, and 500 rpm. The potential was swept negatively from 0.2 to -0.5 V at a scan rate of 50 mV s^{-1}. In addition, the electrode surface was allowed to reach a dynamic steady state for 5 minutes before each test.

2.3 Electrorefining experiment

A three-electrode system was used in the potentiostatic electrorefining experiments, in which the cathode was stainless steel (diameter = 4 mm) , the anode was platinum wire , and the reference electrode was the saturated calomel electrode [24]. During electrorefining, the concentration of Cu^{2+} is 30-50 g L^{-1}, the concentration of H_2SO_4 is 150-250 g L^{-1}, the concentration of Bi^{3+} is 1.5 g L^{-1}, the temperature is 313-333 K, and the electrorefining time is 2 h. The copper obtained by electrorefining was thoroughly rinsed twice with distilled water and dried in an oven filled with Ar gas to prevent surface oxidation before measurements. The copper and bismuth contents in the electrolyte and the products were quantitatively analyzed by EDX-LE and ICP-MS.

3. MATHEMATICAL MODELS

In the flow field of a forced-flowing electrolyte, when the electrolyte polarization is large (η>100 mV), the reaction rate of cations (v) on the electrode surface is given by equation 1:

$$v = \frac{I}{nF} = k^0 C^* A\, exp(-\frac{\alpha nFE}{RT}) \qquad (1)$$

Meanwhile, according to the mass transfer rate equation, the diffusion rate (v') of cations from the bulk solution to the electrode surface is shown in equation 2:

$$v' = k_L A(C_0 - C^*) \qquad (2)$$

In this equation, the mass transfer rate $k_L = \frac{D}{\delta}$, where D is the diffusion coefficient, δ is the thickness of the diffusion layer, C^* is the cation concentration on the electrode surface and C_0 is the bulk solution concentration of cation.

When the electrolysis process reaches an ideal steady state, the reaction rate and diffusion rate of cations reach equilibrium (equation 3):

$$v = k^0 C^* \, exp(-\frac{\alpha nFE}{RT}) = k_L(C_0 - C^*) \qquad (3)$$

The theoretical model (equation 4) can be calculated from the following steps:

First step

$$-V\frac{dC}{dt} = \frac{C}{1/Ak_L + 1/(Ak^0 \, exp(-\frac{\alpha nFE}{RT}))}$$

Second step

$$-\int \frac{1}{C} dc = \frac{1}{V}\int_0^t \frac{1}{1/Ak_L + 1/(Ak^0 \, exp(-\frac{\alpha nFE}{RT}))} dt$$

Third step

$$C(t) = C_0 \, exp(-\frac{1}{V}\int_0^t \frac{1}{1/Ak_L + 1/(Ak^0 \, exp(-\frac{\alpha nFE}{RT}))} dt) \qquad (4)$$

where V is the volume of the electrolyte, A is the exposed area of the electrode, k_L is the function for the flow rate of the solution, k^0 is the reaction rate constant, α is the transfer coefficient, n is the number of transferred electrons, F is the Faraday constant, and E is the electrodeposition potential.

In the flow field of a forced-flowing electrolyte, this mathematical model can be used to reveal the functional relationship between the copper ion concentration variation (C(t)) and electrolysis conditions such as the solution flow rate and polarization potential. Similarly, the relationship between the impurity ion concentration and these electrolysis conditions can also be explained. The diffusion coefficient, the thickness of the diffusion layer, the reaction rate constant and the transfer coefficient can be obtained by using a rotating disk electrode combined with electrochemical tests.

3.1 Determination of model parameters

3.1.1 Diffusion coefficient and the thickness of the diffusion layer

The diffusion coefficients of Cu^{2+} and Bi^{3+} can be determined by measuring the limiting current density when copper and bismuth are deposited on a glassy carbon electrode under different conditions in a forced-flowing electrolyte [25]. The function of the diffusion coefficient's impact on the limiting current density is shown in the following Levich equation (equation 5), and the function presenting diffusion layer thickness based on the diffusion coefficient is shown in equation 6 [22, 26, 27].

$$i_d = 0.62nAFD^{\frac{2}{3}}\nu_1^{-\frac{1}{6}}C^0\omega^{\frac{1}{2}} \qquad (5)$$

$$\delta = 1.61D^{\frac{1}{3}}Y^{\frac{1}{6}}\omega^{-\frac{1}{2}} \qquad (6)$$

where i_d is the cathode limiting current density, n is the number of electrons transferred during the reaction, F is the Faraday constant, A is the surface area of the electrode, D is the diffusion coefficient,

ω is the rotating angular velocity, v is the kinematic viscosity of the electrolyte, Y is the dynamic viscosity of the electrolyte, and C^0 is the bulk concentration of cations.

Fig. 1 shows the linear voltammetry curves of Cu^{2+} and Bi^{3+}. Under different Cu^{2+} concentrations, the limiting current density plateau of Cu^{2+} appears at a potential of approximately -0.35 V, and 1.5 g L^{-1} Bi^{3+} appears at approximately -0.1V.

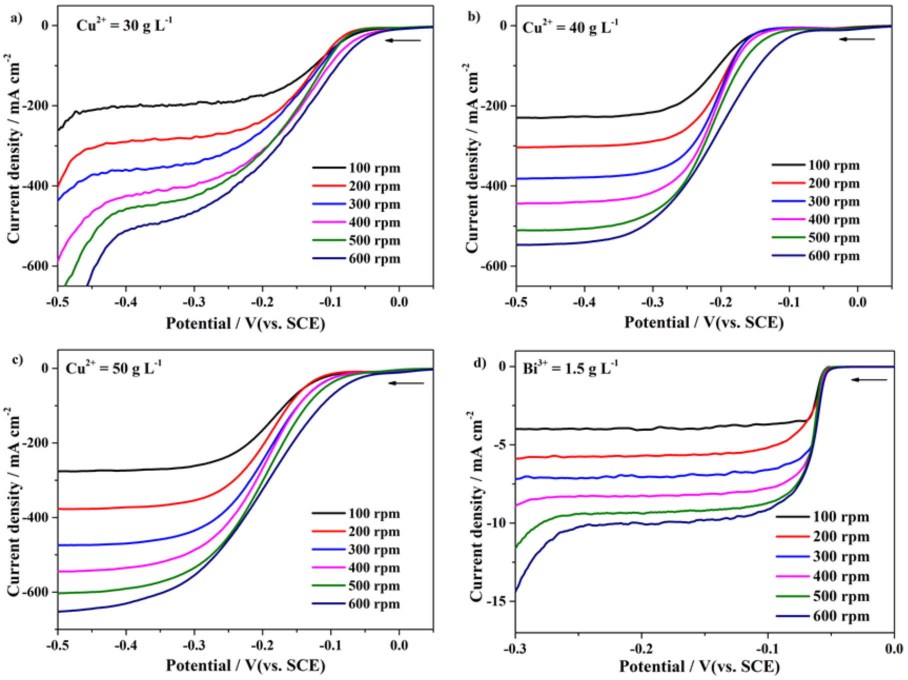

Figure 1. The linear voltammetry curves of Cu^{2+} and Bi^{3+}. (T = 323 K, H_2SO_4 = 200 g L^{-1}, 500 rpm)

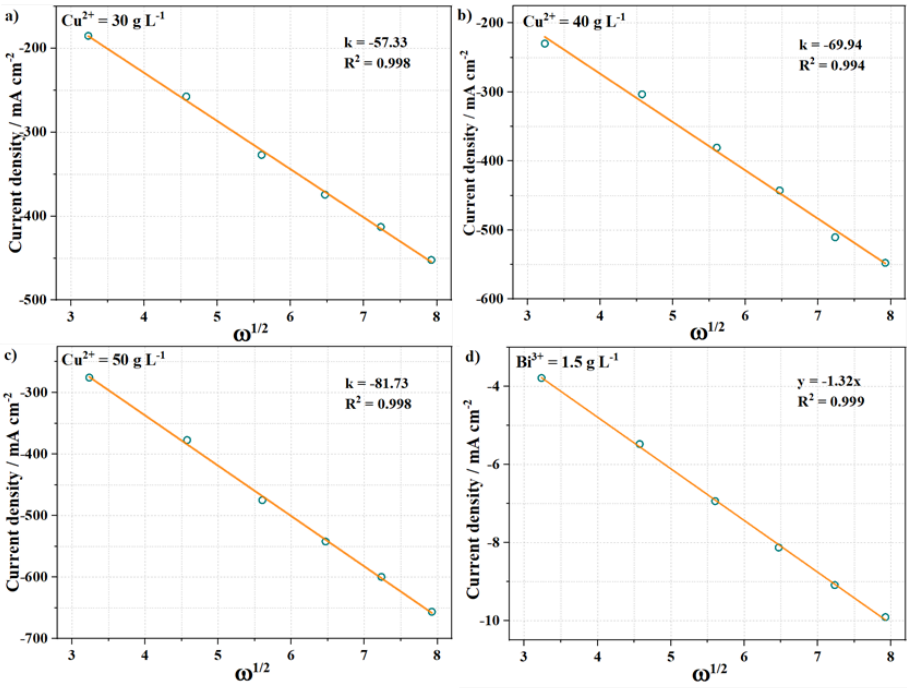

Figure 2. i-$\omega^{1/2}$ diagrams of Cu^{2+} and Bi^{3+}. (T = 323 K, H_2SO_4 = 200 g L^{-1}, 500 rpm)

Fig. 2 shows the relationship between the limiting current density (*i*) and the corresponding rotating speed (*w*) obtained from Fig. 1. Both i and $\omega^{1/2}$ of Cu^{2+} and Bi^{3+} show a linear relationship. Based on the line slope, the corresponding diffusion coefficient and the thickness of the diffusion layer can be calculated.

3.1.2 Reaction rate constant and transfer coefficient

Important kinetic parameters, such as the reaction rate constant (k^0) and the transfer coefficient (α), can be calculated by Tafel curves using equations 7 and 8 [28, 29].

$$i^0 = nFC_0k^0\exp(-\frac{\alpha nFE}{RT}) \qquad (7)$$

$$\alpha n = \frac{2.303RT}{k} \qquad (8)$$

where k is the slope of the dotted line shown in the Fig. 3.

Fig. 3 shows the Tafel curves of Cu^{2+} and Bi^{3+} reduction at the cathode. Through the extrapolation method, the corresponding exchange current density (i^0) were inferred. Then, the reaction rate constant and the transfer coefficient were acquired. These three parameters were used to reveal the difficulty of reducing copper and impurity ions under different conditions. For example, as the concentration of Cu^{2+} increases, the exchange current density increases accordingly, that is, the driving force required for reduction decreases, and the deposition of copper becomes easier.

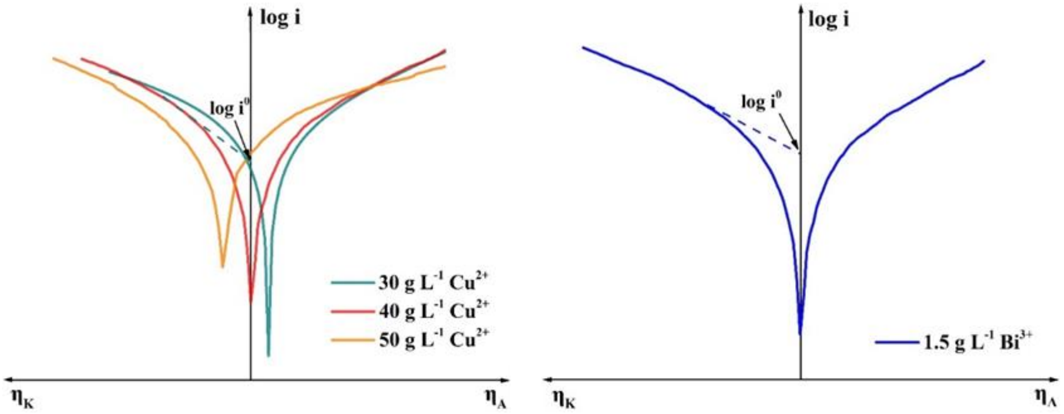

Figure 3. Tafel curves of Cu^{2+} and Bi^{3+}. (T = 323 K, H_2SO_4 = 200 g L^{-1}, 500 rpm)

4. RESULTS AND DISCUSSION

4.1 The influence of various factors on the cathode copper purity with the theoretical model

In the copper electrolyte containing bismuth impurities, the reduction process of Cu^{2+} and Bi^{3+} under different temperatures, electrode speeds and other electrolysis conditions was investigated by a rotating disk electrode. The influence of bismuth on the theoretical composition of deposited copper was calculated according to the theoretical model. The electrolyte with a high concentration of bismuth was used in the theoretical study to better understand the effect of bismuth impurities on copper purity. Electrorefining experiments were carried out to define the accuracy of the model. In addition, electrorefining experiments in simulated industrial electrolytes were also conducted to verify the applicability of the model under complex conditions.

4.1.1 Influence of different initial copper concentration

Table 1 shows the D, δ, k^0 and αn of Cu^{2+} and Bi^{3+} as calculated by equations 5, 6, 7 and 8 in the flow field of the forced-flowing electrolyte. As the Cu^{2+} concentration increases, the diffusion coefficient of Cu^{2+} decreases slightly. This is consistent with the conclusion given by Michael [30]. Meanwhile, as the concentration increases, αn shows an upward trend because the higher bulk concentration makes it easier for Cu^{2+} to migrate to the electrode surface.

Table 1. D, δ, k^0 and αn of Cu^{2+} and Bi^{3+} under different initial Cu^{2+} concentrations. (T = 323 K, H_2SO_4 = 200 g L^{-1}, 500 rpm)

C (g L^{-1})	D (cm^2 s^{-1})	δ (cm)	k^0 (cm s^{-1})	αn
Cu = 30	9.37×10^{-6}	2.19×10^{-3}	0.398	0.76
Cu = 40	9.20×10^{-6}	2.17×10^{-3}	1.003	0.87
Cu = 50	8.57×10^{-6}	2.17×10^{-3}	1.775	0.95
Bi = 1.5	9.03×10^{-6}	2.07×10^{-3}	0.0827	0.75

The above data are substituted into the theoretical model (equation 4), and the corresponding Cu^{2+} and Bi^{3+} concentrations at different times are shown in Fig. 4.

With increasing initial Cu^{2+} concentration, the deposition rate of Cu^{2+} increased from 0.182 g h^{-1} to 0.246 g h^{-1}. As the ion concentration in the bulk solution rises, the ion concentration on the electrode surface also increases, resulting in the affect of ion mass transfer on the cathodic reduction rate being weakened. The control step determining the reaction rate gradually shifts from diffusion control to charge control, leading to an accelerated deposition rate [31, 32].

Fig. 5 shows the theoretical composition of deposited copper at different initial Cu^{2+} concentrations. (The initial concentration of Bi^{3+} is 1.5 g L^{-1}). It can be concluded that as the initial concentration of Cu^{2+} increases from 30 g L^{-1} to 50 g L^{-1}, the purity of the cathode copper increases by 0.30%. Based on the analysis of Table 1, the increase in the Cu^{2+} concentration significantly increases αn and k^0. Furthermore, the rise of Cu^{2+} concentration in the bulk solution significantly increases the Cu^{2+} concentration on the electrode surface, and causes the potential required for deposition to move forward according to the Nernst equation (equation 9), resulting in a decrease of the electrodeposition resistance.

$$\varphi_{M^{n+}/M} = \varphi^0_{M^{n+}/M} + \frac{RT}{nF} ln[M^{n+}] \qquad (9)$$

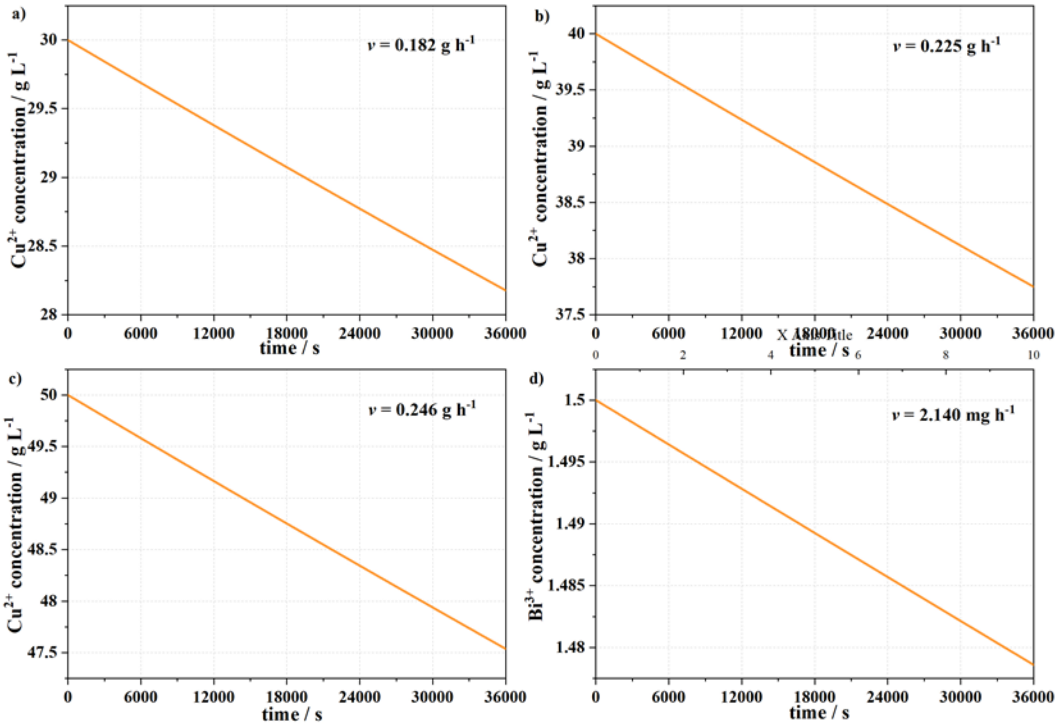

Figure 4. Theoretical Cu^{2+} and Bi^{3+} concentration with time under different initial Cu^{2+} concentrations. (a) Cu^{2+} = 30 g L^{-1}, b) Cu^{2+} = 40 g L^{-1}, c) Cu^{2+} = 50 g L^{-1}, d) Bi^{3+} = 1.5 g L^{-1}, T = 323 K, H_2SO_4 = 200 g L^{-1}, 500 rpm, E = 0.01 V)

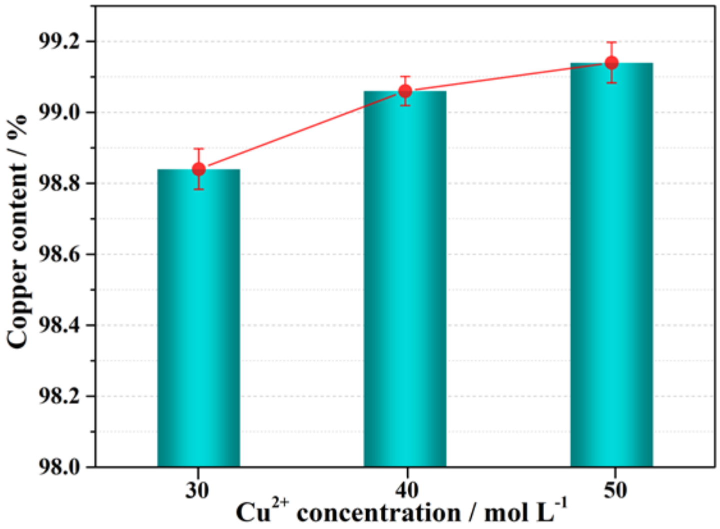

Figure 5. Theoretical composition of deposited copper under different initial copper concentrations. (Bi = 1.5 g L^{-1}, T = 323 K, H_2SO_4 = 200 g L^{-1}, 500 rpm, E = 0.01 V)

Therefore, Cu^{2+} is easier to reduce at the cathode. In summary, actual electrorefining should be carried out in an electrolyte with a Cu^{2+} concentration higher than 40 g L^{-1}, and the electrolyte should be replenished regularly to maintain the Cu^{2+} concentration at a high level.

4.1.2 Influence of different temperature

Table 2 shows the D, δ, k^0 and αn of Cu^{2+} and Bi^{3+} at different temperatures calculated by equations 5, 6, 7 and 8 in the flow field of the forced-flowing electrolyte. Table 2 shows that the diffusion coefficient of Cu^{2+} and Bi^{3+} increases with increasing temperature [30], and that high temperatures can significantly accelerate the diffusion rate of ions in the electrolyte [33]. However, it can also be observed that the transfer coefficient of Cu^{2+} decreases when the temperature is higher than 323 K.

Table 2. D, δ, k^0 and αn of Cu^{2+} and Bi^{3+} at different temperatures. (Cu = 30 g L^{-1}, Bi = 1.5 g L^{-1}, H_2SO_4 = 200 g L^{-1}, 500 rpm, E = 0.01 V)

T K	Cu				Bi			
	D × 10^{-6} (cm^2 s^{-1})	δ × 10^{-3} (cm)	k^0 (cm s^{-1})	αn	D × 10^{-6} (cm^2 s^{-1})	δ × 10^{-3} (cm)	k^0 (cm s^{-1})	αn
313	7.26	2.06	0.159	0.67	7.87	2.04	0.0588	0.64
318	8.43	2.13	0.286	0.72	8.37	2.05	0.0692	0.69
323	9.37	2.17	0.398	0.80	9.03	2.07	0.0827	0.75
328	10.18	2.21	0.549	0.78	9.62	2.09	0.1019	0.81
333	11.76	2.23	0.724	0.77	10.40	2.11	0.1241	0.86

By substituting the data in Table 2 into the theoretical model (equation 4), the relationship between the concentrations of Cu^{2+} and Bi^{3+} and time is calculated at different temperatures, as shown in Fig. 6. As the temperature rises, the deposition rate of Cu^{2+} first increases and then decreases; the reduction rate is the fastest at approximately 323 K. For Bi^{3+}, the deposition rate increases monotonically with increasing temperature. The reduction rate of Cu^{2+} decreased after the temperature increased past 323 K, which was most likely due to the amount of Cu^{2+} diffusing to the electrode surface reaching the limit of electrochemical reduction at high temperature. Currently, the reduction rate of Cu^{2+} is less affected by the liquid phase mass transfer process, and the charge transfer step becomes the rate-determining step of the reduction. In addition, when the temperature is higher than 323 K, the transfer coefficient of Cu^{2+} decreases; in other words, the activation energy required for the reduction increases, and the reduction of Cu^{2+} becomes difficult.

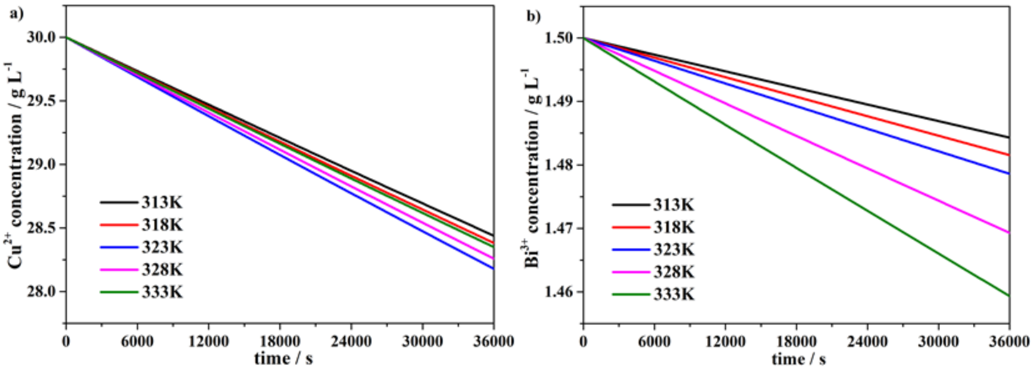

Figure 6. Theoretical curves of Cu^{2+} and Bi^{3+} concentration with time at different temperatures. (a) Cu = 30 g L^{-1}; b) Bi = 1.5 g L^{-1}, H_2SO_4 = 200 g L^{-1}, 500 rpm, E = 0.01 V)

Fig. 7 shows the theoretical composition of deposited copper at different temperatures. As shown in Fig. 7, with increasing temperature, the purity of copper decreases, from 99.00% at 313 K to 98.38% at 333 K. When the temperature was lower than 323 K, it had little impact on the purity, but when the temperature was higher than 323 K, the copper purity dropped rapidly. This happened was mainly because the reduction rate of copper decreased while the reduction rate of bismuth increased. Simultaneously, the rise of temperature possibly also accelerates the dissolution rate of the cathode copper , resulting in a decrease in the deposition amount and purity of copper. Because a low temperature will affect the solubility of copper in the electrolyte and the production efficiency of electrorefining, 323 K is the most suitable electrolysis temperature.

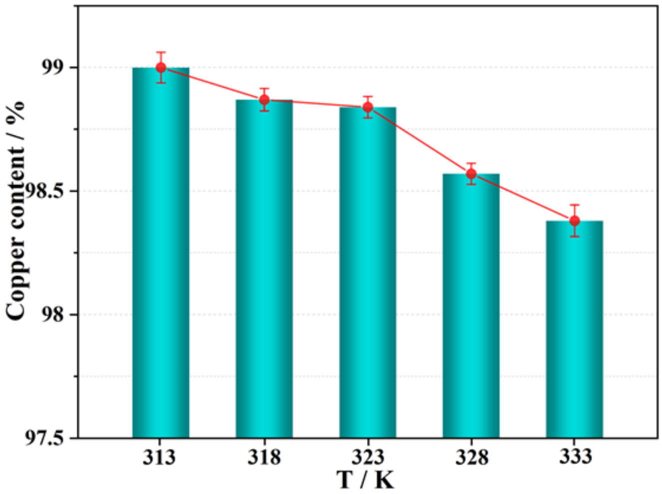

Figure 7. Theoretical composition of deposited copper at different temperatures. (Cu = 30 g L^{-1}, Bi = 1.5 g L^{-1}, H_2SO_4 = 200 g L^{-1}, 500 rpm, E = 0.01 V)

4.1.3 Influence of different electrode rotating speeds

Table 3. δ, k^0 and αn of Cu^{2+} and Bi^{3+} under different electrode rotating speeds. (Cu = 30 g L^{-1}, Bi = 1.5 g L^{-1}, T = 323 K, H_2SO_4 = 200 g L^{-1}, E = 0.01 V)

Speed rpm	Cu			Bi		
	δ × 10^{-3} (cm)	k^0 (cm s^{-1})	αn	δ × 10^{-3} (cm)	k^0 (cm s^{-1})	αn
100	4.86	2.578	0.95	4.63	13.37	1.26
200	3.44	1.886	0.91	3.28	3.056	1.11
300	2.81	0.971	0.85	2.68	0.732	0.97
400	2.43	0.589	0.80	2.32	0.589	0.86
500	2.17	0.398	0.76	2.17	0.0827	0.75

Table 3 shows the δ, k^0 and αn of Cu^{2+} and Bi^{3+} at different electrode rotating speeds as calculated by equations 5, 6, 7 and 8 in the flow field of the forced-flowing electrolyte. Among them,

D_{Cu}=9.37×10^{-6} mA cm^{-2}, D_{Bi}=9.03×10^{-6} mA cm^{-2}. With increasing electrode rotating speed, the thickness of the diffusion layer of Cu^{2+} and Bi^{3+} decreases significantly, indicating that their diffusion resistance is reduced. However, the increase in rotational speed also leads to a decline in the transfer coefficient, which may be attributed to the convection of the solution and the destruction of the double layer on the electrode surface at a higher rotating speed, which results in a decrease in the apparent concentration of ions in the solution. The activation energy needed for reduction is increased.

The Cu^{2+} and Bi^{3+} concentrations shown at different times are shown in Fig. 8 and were found by substituting the data of different electrode rotating speeds in Table 3 into the theoretical model (equation 4). It can be observed that with the continuous increase of the rotating speed during electrorefining, the deposition rate of Cu^{2+} first rises first and then decreases while the deposition rate of Bi^{3+} always shows a downward trend. The increase in rotational speed can accelerate the migration of Cu^{2+} and Bi^{3+} in the bulk solution but can also lead to the reaction rate constant of the two ions decreasing continuously, which might also be caused by the negative reaction of hydrogen evolution on the electrode surface. At the same time, a high rotational speed decreases the transfer coefficient of the two ions, and increases the activation energy required for the reduction. The combined influence of the above factors eventually leads to a slower deposition rate of Cu^{2+} and Bi^{3+} at a higher electrode rotating speed.

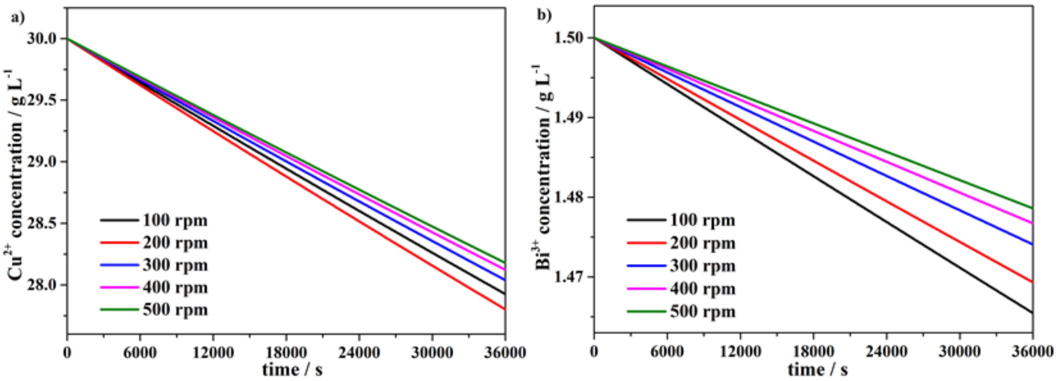

Figure 8. Theoretical curves of Cu^{2+} and Bi^{3+} concentration with time under different electrode rotating speeds. (a) Cu = 30 g L^{-1}; b) Bi = 1.5 g L^{-1}, T = 323 K, H_2SO_4 = 200 g L^{-1}, E = 0.01 V)

Fig. 9 shows the theoretical composition of deposited copper at different electrode rotating speeds. With increasing rotating speed, the purity of the copper product continuously increases, from 98.36% at 100 rpm to 98.84% at 500 rpm. In other words, a higher electrode rotation speed during deposition slightly hinders copper deposition, but the inhibition effect on Bi^{3+} is greater, which is helpful to improve the purity of the copper. In actual electrorefining, it is ideal to control the speed at approximately 400 rpm or keep the solution flow rate at an equivalent level.

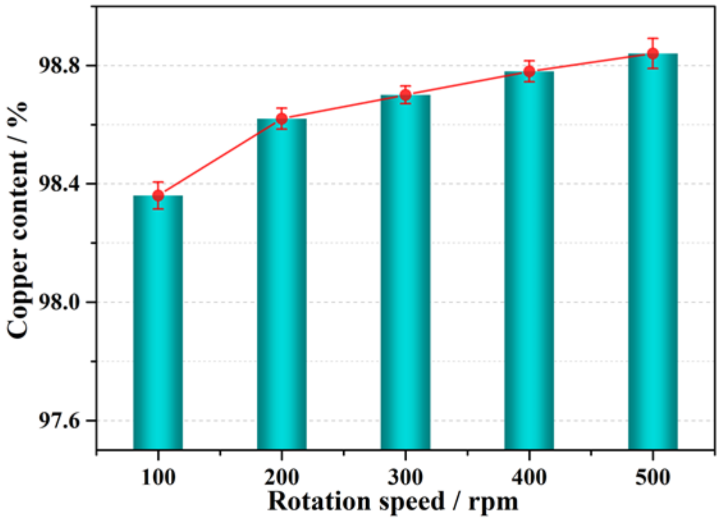

Figure 9. Theoretical composition of deposited copper under different electrode rotation speeds. (Cu = 30 g L^{-1}, Bi = 1.5 g L^{-1}, T = 323 K, H_2SO_4 = 200 g L^{-1}, E = 0.01 V)

4.1.4 Influence of different H_2SO_4 concentration

Table 4 shows the D, δ, k^0 and αn of Cu^{2+} and Bi^{3+} at different H_2SO_4 concentrations as calculated by equations 5, 6, 7 and 8 in the flow field of the electrolyte. Table 4 shows that with increasing sulfuric acid concentration, the diffusion coefficients of Cu^{2+} and Bi^{3+} decrease, but the thickness of the diffusion layer remains practically constant. Michael [30] found that increasing the sulfuric acid concentration from 160 g L^{-1} to 200 g L^{-1} reduced the diffusion rate of copper ions by 20%. The increase in sulfuric acid concentration may cause the viscosity of the electrolyte to increase greatly, which makes diffusion difficult [34].

Table 4. D, δ, k^0 and αn of Cu^{2+} and Bi^{3+} under different H_2SO_4 concentrations. (Cu = 30 g L^{-1}, Bi = 1.5 g L^{-1}, T = 323 K, H_2SO_4 = 200 g L^{-1}, E = 0.01 V)

$c(H_2SO_4)$ g L^{-1}	Cu				Bi			
	D × 10^{-6} (cm^2 s^{-1})	δ × 10^{-3} (cm)	k^0 (cm s^{-1})	αn	D × 10^{-6} (cm^2 s^{-1})	δ × 10^{-3} (cm)	k^0 (cm s^{-1})	αn
150	9.77	2.18	0.207	0.74	9.57	2.08	0.0493	0.70
200	9.37	2.17	0.398	0.76	9.03	2.07	0.0827	0.75
250	9.09	2.18	0.454	0.83	8.49	2.06	0.1472	0.78

The Cu^{2+} and Bi^{3+} concentrations at different times corresponding to the data of different H_2SO_4 concentrations in Table 4 being substituted into the theoretical model (equation 4), are shown in Fig. 10. It is obvious that the changes in the Cu^{2+} and Bi^{3+} reduction rates are different. For Cu^{2+}, when the sulfuric acid concentration was 200 g L^{-1}, the reduction rate was the fastest, while the reduction rate of

Bi^{3+} increased with increasing sulfuric acid concentration. Combined with Table 4, it can be seen that within the adopted H_2SO_4 concentration range, the reaction rate constant and transfer coefficient of the two cations both increase; that is, a high H_2SO_4 concentration can promote the reduction of Cu^{2+} and Bi^{3+} [35]. However, when the H_2SO_4 concentration increases from 200 g L^{-1} to 250 g L^{-1}, the reaction rate constant of Cu^{2+} only has a small change, indicating that there is a strong hydrogen evolution side reaction in the electrolyte, which affects the reduction of Cu^{2+}. In addition, at this time, the viscosity of the electrolyte is high, so the generated hydrogen cannot quickly separate from the electrode, which hinders the reduction of Cu^{2+}. For Bi^{3+} with a lower concentration, fewer sites are required for discharge reduction on the cathode surface, and the reaction rate is less affected by the hydrogen evolution reaction.

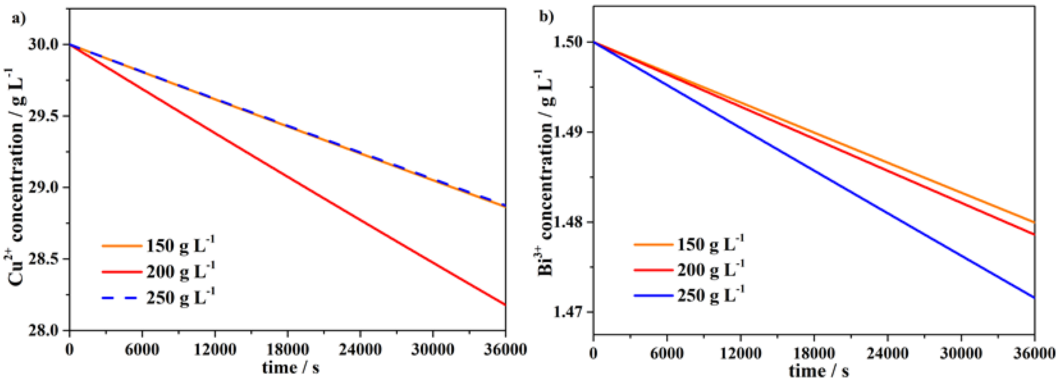

Figure 10. Theoretical curves of Cu^{2+} and Bi^{3+} concentration with time under different H_2SO_4 concentrations. (a) Cu = 30 g L^{-1}; b) Bi = 1.5 g L^{-1}, T = 323 K, 500rpm, E = 0.01 V)

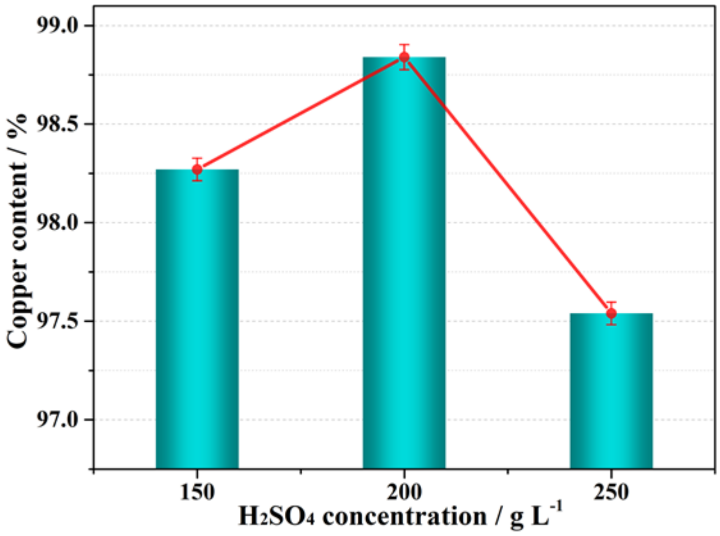

Figure 11. Theoretical composition of deposited copper under different H_2SO_4 concentrations. (Cu = 30 g L^{-1}, Bi = 1.5 g L^{-1}, T = 323 K, 500 rpm, E = 0.01 V)

Fig. 11 shows theoretical composition of deposited copper under different H_2SO_4 concentrations. Obviously, the copper obtained when H_2SO_4 was 200 g L^{-1} had the highest purity. Compared with 250 g L^{-1} H_2SO_4, the theoretical composition of deposited copper can be increased by 1.3%. The purity of copper obtained in 150 g L^{-1} H_2SO_4 was also better than 250 g L^{-1}. Therefore, the H_2SO_4 concentration should not be too high in actual electrorefining; approximately 200 g L^{-1} is appropriate.

4.1.5 Influence of different deposition potential

Fig. 12 shows the theoretical curves of the Cu^{2+} and Bi^{3+} concentrations at different times calculated by the theoretical model under different deposition potentials. It can be concluded that when the potential is negatively shifted during deposition, the deposition rates of Cu^{2+} and Bi^{3+} are both accelerated significantly, which is attributed to the greater driving force for reduction at a more negative potential.

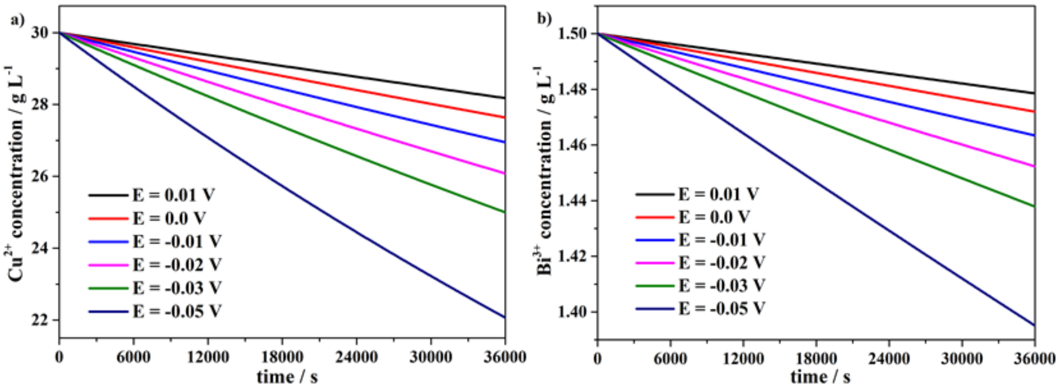

Figure 12. Theoretical curves of the Cu^{2+} and Bi^{3+} concentrations under different deposition potentials. (a) Cu = 30 g L^{-1}; b) Bi = 1.5 g L^{-1}, T = 323 K, H_2SO_4 = 200 g L^{-1}, 500 rpm)

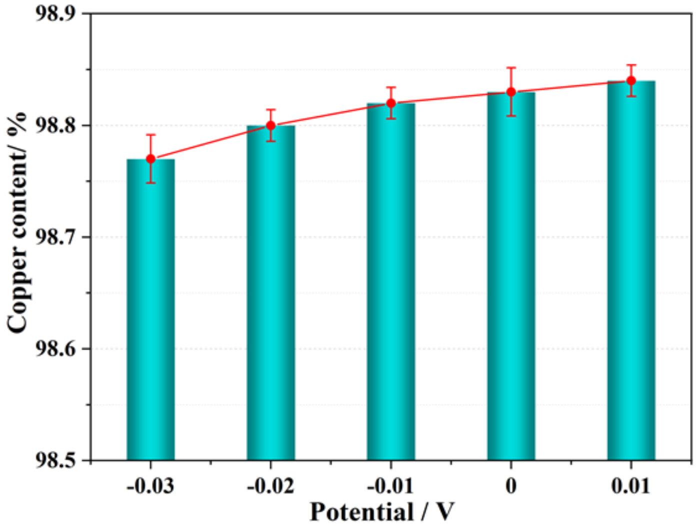

Figure 13. Theoretical composition of deposited copper under different deposition potentials. (Cu = 30 g L^{-1}, Bi = 1.5 g L^{-1}, T = 323 K, H_2SO_4 = 200 g L^{-1}, 500 rpm)

Fig. 13 shows the theoretical composition of deposited copper at different electrode rotating speeds. As the deposition potential shifts negatively, the purity of the copper gradually decreases. At this time, both Cu^{2+} and Bi^{3+} obtain a larger reduction driving force, in other words, they have a faster reduction rate, resulting in an increase of the Cu^{2+} depleted area on the electrode surface, more Bi^{3+} can be reduced at the cathode. And the copper reduction rate is affected by the side reaction of hydrogen evolution at a relatively negative potential, which reduces the copper purity [36].

In actual industrial electrorefining processes, a more positive potential should be selected for electrorefining. However, an excessively positive potential also leads to a deceleration of the deposition rate, eventually affecting the production efficiency of copper electrorefining. Therefore, it is appropriate to control the deposition potential between -0.01~0.01 V.

4.2 Experimental verification of the theoretical model

The effects of temperature, rotation speed and deposition potential on the theoretical composition of deposited copper were analyzed by a theoretical model. The results indicate that the higher Cu^{2+} concentration and rotating speed, the lower temperature and deposition potential are beneficial for obtaining high-purity cathode copper, while a sulfuric acid concentration of 200 g L^{-1} is the most favorable to improve the purity of copper. To verify the validity of the theoretical model, electrorefining experiments were carried out under the corresponding conditions.

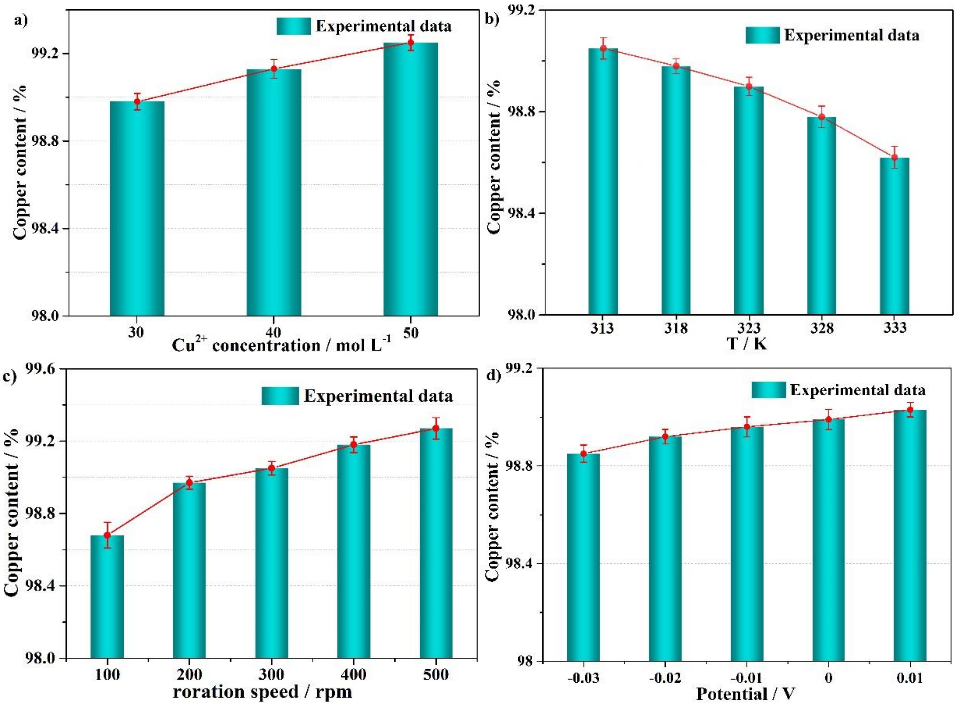

Figure 14. Variation in composition of deposited copper during actual electrorefining (a) Bi = 1.5 g L^{-1}, T = 323 K, H_2SO_4 = 200 g L^{-1}, 500 rpm; b) Cu = 30 g L^{-1}, Bi = 1.5 g L^{-1}, H_2SO_4 = 200 g L^{-1}, 500 rpm, E = 0.01 V; c) Cu = 30 g L^{-1}, Bi = 1.5 g L^{-1}, T = 323 K, H_2SO_4 = 200 g L^{-1}, E = 0.01 V; d) Cu = 30 g L^{-1}, Bi = 1.5 g L^{-1}, T = 323 K, H_2SO_4 = 200 g L^{-1}, 500 rpm)

Fig. 14 shows the variation in the cathode copper purity during electrorefining. Under the same conditions, the change rule of copper purity in the actual electrorefining process is consistent with that obtained by the above theoretical model, which means that the model can effectively reflect the change in copper purity after electrorefining.

At the same time, the applicability of the theoretical model to industrial electrolytes was verified. Combined with the above experimental results, the electrorefining experiments were carried out in the industrial electrolyte using the optimal process given by the theoretical model. The obtained products were dissolved in nitric acid for ICP-MS detection. The results are shown in Table 5. The Cu^{2+} concentration in the electrolyte decreases from 40 g L^{-1} to 37.96 g L^{-1} and 37.31 g L^{-1} after 10 h electrolysis, which is almost consistent with the calculated Cu^{2+} concentration of 37.75 g L^{-1}. It is worth mentioning that the purity of copper can reach 99.995% in electrolytes with high impurities. Overall, the optimal process given by the theoretical model is also suitable for industrial electrolyte systems and can effectively predict the change in ion concentration in different copper electrolytes to obtain the optimal electrolysis conditions for the preparation of high purity cathode copper.

Table 5. Electrolyte composition and actual cathode copper purity (T = 323 K, H_2SO_4 = 200 g L^{-1}, 400 rpm, E = 0.01 V)

No.	Electrolyte composition (g L^{-1})					10 h electrolysis (g L^{-1})	Copper purity (%)
	Cu	As	Sb	Bi	Ni	Cu (theory/actual)	
1	40	12	0.6	0.4	10	37.75/37.96	99.984
2	40	8	0.2	0.2	10	37.75/37.31	99.991
3	50	8	0.6	0.2	10	47.54/47.18	99.995

5. CONCLUSIONS

In the flow field of the forced-flowing electrolyte, the influence of the temperature, H_2SO_4 concentration, deposition potential and other electrolysis factors on the cation reduction rate was determined based on diffusion layer theory. A theoretical model was established, which can be used to predict the rules for changes in Cu^{2+} and Bi^{3+} concentrations in different electrolysis conditions during electrorefining. The most favorable conditions for the deposition of Cu^{2+} according to the theoretical model and for minimizing the precipitation of Bi^{3+} were found to be 323 K, 400-500 rpm, 200 g L^{-1} H_2SO_4 and a relatively positive potential . Electrorefining experiments confirmed that the change rule of copper purity under the same conditions is consistent with the theoretical model, indicating that the model can be used in electrorefining processes. Based on theoretical research, copper electrorefining experiments that simulate industrial electrolysis were carried out, and the results showed that the change in Cu^{2+} was consistent with the results obtained by the theoretical model. The purity of copper reached 99.995% when Cu was 50 g L^{-1}, Ni was 10 g L^{-1} and As, Sb, and Bi were 8, 0.6, and 0.2 g L^{-1}, respectively. This paper provides effective guidance for industrial copper electrorefining.

ACKNOWLEDGEMENT
This work was financially supported by the Natural Science Foundation of Zhejiang Province (No. LY17B030009) and Science and Technology Research Project of Keqiao, Zhejiang (No. 2021JBGS208).

References

1. P. Coursol, P.J. Mackey, J.P.T. Kapusta, N.C. Valencia, *JOM*, 67 (2015) 1066.
2. M. Bacedoni, I. Moreno-Ventas, G. Ríos, *Metals*, 10 (2020) 1229.
3. X. Jiang, Z. Cui, M. Chen, B. Zhao, *Metall. Mater. Trans. B.*, 50 (2018) 173.
4. Y. Chen, *Int. J. Manuf. Technol. Manag.*, 25 (2012) 224.
5. K. Song, A. Jokilaakso, *Min. Proc. Ext. Met. Rev.*, (2020) 1.
6. O. Forsén, J. Aromaa, M. Lundström, *Recycling*, 2 (2017) 219.
7. S. Ishihara, K. Shinoda, J. Kano, *Minerals*, 9 (2019) 349.
8. J.H. Liu, W.H. Gui, Y.F. Xie, C.H. Yang, *Appl. Math. Model.*, 38 (2014) 2206.
9. X. Wang, Q. Chen, Z. Yin, M. Wang, B. Xiao, F. Zhang, *Hydrometallurgy*, 105 (2011) 355.
10. X.W. Wang, Q.Y. Chen, Z.L. Yin, M.Y. Wang, F. Tang, *Hydrometallurgy*, 108 (2011), 199.
11. S. Jafari, M. Kiviluoma, T. Kalliomäki, E. Klindtworth, A.T. Aji, J. Aromaa, B.P. Wilson, M. Lundström, *Int. J. Miner. Process.*, 168 (2017) 109.
12. F.X. Xiao, D. Cao, J.W. Mao, *T. Nonferr. Metal. Soc.*, 24 (2014) 271.
13. W. Zeng, S. Wang, M.L. Free, *JOM*, 69 (2016) 1876.
14. J.Y. Li, T. Wang, Z.H. Sun, J.J. Wu, D.L. Shen, Q. Yuan, X.X. Li, J. Chen, *Sep. Purif. Technol.*, 199 (2018) 282.
15. B. Li, X. Wang, Y. Wei, W. Hua, B. Mansoor, *Miner. Eng.*, 128 (2018) 247.
16. S. Zhou, *Nonferr. Metal.*, (2008) 1. (in chinese)
17. S. Wang, *JOM*, 60 (2008) 41.
18. M. Strawski, M. Szklarczyk, *J. Electroanal. Chem.*, 641 (2010) 23.
19. B. Yu, R. Xu, Y. Li, J. Zhang, Z. Qin, *Int. J. Electrochem. Sci*, 12 9(2017) 8059.
20. V.M. Volgin, A.D. Davydov, *Russ. J. Electrochem.*, 56 (2020) 785.
21. L.A. Diaz, G.G. Botte, *Electrochim Acta*, 179 (2015) 519.
22. T. Kalliomäki, B.P. Wilson, J. Aromaa, M. Lundström, *Miner. Eng.* 134 (2019) 381.
23. D.A. Dudek, P.S. Fedkiw, *J. Electroanal. Chem.*, 474 (1999) 16.
24. F. Verbruggen, E. Fiset, L. Bonin, A. Prévoteau, M.S. Moats, T. Hennebel, K. Rabaey, *J. Appl. Electrochem.*, 51 (2021) 219.
25. R. Schmidt, J. Gaida, *Chemelectrochem*, 4 (2017) 1849.
26. Q.K. Zhuang, H.Y. Chen, *Electroanal.*, 6 (1994) 485.
27. A.N. Oldacre, E.R. Young, *RSC Adv.*, 10 (2020) 14804.
28. P. Khadke, T. Tichter, T. Boettcher, F. Muench, C. Roth, *Sci. Rep.*, 11 (2021) 8974.
29. K.B. Oldham, J.C. Myland, C.G. Zoski, A.M. Bond, *J. Electroanal. Chem. Interfa. Electrochem.*, 270 (1989) 79.
30. M.S. Moats, J.B. Hiskey, D.W. Collins, *Hydrometallurgy*, 56 (2000) 255.
31. A. Kuleyin, H. E. Uysal, *Int. J. Electrochem. Sci*, 15 (2020) 1474.
32. M. Rezaei, S.H. Tabaian, D.F. Haghshenas, *J. Electroanal. Chem.*, 687 (2012) 95.
33. E. Stricker, Z. Adler, J. Wainright, R. Savinell, *J. Chem. Eng. Data*, 64 (2019) 1095.

34. T. Kalliomaki, A.T. Aji, L. Rintala, J. Aromaa, M. Lundstrom, *Physicochem. Probl. Mi.*, 53 (2017) 1023.
35. S.M. Rosa-Ortiz, F. Khorramshahi, A. Takshi, *J. Appl. Electrochem.*, 49 (2019) 1203.
36. M. Rezaei, S.H. Tabaian, D.F. Haghshenas, *Electrochim. Acta*, 87 (2013) 381.